Continuous Trailing-Edge Flaps for Primary Flight Control of a Helicopter Main Rotor

Robert P. Thornburgh
robert.p.thornburgh.civ@mail.mil
Research Engineer

Andrew R. Kreshock
andrew.r.kreshock.civ@mail.mil
Research Engineer

Matthew L. Wilbur
matthew.l.wilbur.civ@mail.mil
Sr. Research Engineer

U.S. Army Research Laboratory
Vehicle Technology Directorate
Hampton, Virginia

Martin K. Sekula
martin.k.sekula@nasa.gov
Sr. Research Engineer
NASA Langley Research Center
Hampton, Virginia

Jinwei Shen
Research Engineer
National Institute of Aerospace
Hampton, Virginia

ABSTRACT

The use of continuous trailing-edge flaps (CTEFs) for primary flight control of a helicopter main rotor is studied. A practical, optimized bimorph design with Macro-Fiber Composite actuators is developed for CTEF control, and a coupled structures and computational fluid dynamics methodology is used to study the fundamental behavior of an airfoil with CTEFs. These results are used within a comprehensive rotorcraft analysis model to study the control authority requirements of the CTEFs when utilized for primary flight control of a utility class helicopter. A study of the effect of blade root pitch index (RPI) on CTEF control authority is conducted, and the impact of structural and aerodynamic model complexity on the comprehensive analysis results is presented. The results show that primary flight control using CTEFs is promising; however, a more viable option may include the control of blade RPI, as well.

INTRODUCTION

Active control of helicopter rotor systems has been studied extensively by research organizations in government, industry, and academia for nearly 40 years. The primary goals of these studies have been to reduce rotorcraft noise and vibration, and/or to improve rotorcraft performance, range, and payload. Numerous concepts have been analyzed, studied, and developed to meet these objectives; however, the rotorcraft community has yet to identify a concept that is considered sufficiently successful to be adopted by a major rotorcraft manufacturer for implementation in their aircraft. Evidence exists of some fielded fixed-frame active control devices, but these usually provide significantly reduced control authority as compared to the rotor-system-based active control methods that attack the problems of interest at their source. For active rotor control systems to be adopted in the future, breakthrough technologies will need to be developed that significantly 1) reduce the cost of implementing active rotor control devices, 2) improve active control device reliability and ease of manufacture, and 3) eliminate safety concerns regarding the use of active rotor controls. In short, such a future device will have to "buy its way onto the aircraft" by providing a solution that is less costly to implement than currently fielded technologies while offering a significant improvement in rotorcraft performance through improved range, payload, fuselage vibration reduction, and/or acoustic signature reduction. While most of the active rotor technologies developed over the years offer unquestionable advantages in terms of rotorcraft performance, the cost of implementation has yet to reach a sufficiently low level to justify their use on production aircraft. This paper will present an active rotor control concept that seeks to minimize the amount of active control devices used on the blade, while offering a low-drag alternative to the conventional swashplate rotor control system.

The active rotor control method presented herein utilizes continuous trailing-edge flaps (CTEFs) to provide primary flight control for a conventional rotorcraft flight vehicle sized to meet typical utility helicopter mission requirements. The CTEF concept (ref. 1) uses embedded

Presented at the AHS 70th Annual Forum, Montréal, Québec, Canada, May 20–22, 2014.

active materials internal to the airfoil section to distort the trailing-edge section in a static or dynamic fashion. Such displacement is used to effect changes in the basic lift and pitching moment characteristics of the airfoils, while minimizing the impact on drag. The CTEF approach eliminates mechanical linkages and flap hinges in the rotating system, as would be required in a discrete trailing-edge flap implementation, thus minimizing drag while maintaining sufficient control authority. This concept is similar to the Active Trailing Edge presented in reference 2, but the CTEF design distributes the deformation over a larger chord length and results in a smoother aerodynamic profile. The development of an optimized CTEF design was explored in reference 3, resulting in structural design requirements to maximize trailing-edge deflections. The influence of aerodynamic loads on CTEF displacement was considered, and analysis indicated that the amount of control authority available from CTEF deflection may be sufficient to provide primary flight control.

A number of authors have investigated trailing-edge flaps as a method for providing primary flight-control in swashplateless helicopter rotors (refs. 4-10). However, these investigations have all used traditional hinged flaps rather than airfoils with deformable cross-sections. The primary challenge that has been identified is that current on-blade actuators are unable to provide adequate flap deflections to maintain rotor trim throughout the entire flight envelope. Recent work has addressed this issue through the use of separate flaps for the collective and cyclic controls (refs. 9-10). The current study builds on this work, utilizing two radial CTEF regions per blade, one collective and one cyclic, to provide primary flight control. In addition, control of the collective pitch through changes in the blade root pitch index is examined.

Thus, the objective of this paper is to explore the feasibility of utilizing CTEFs to provide primary flight control for the main rotor of a conventional helicopter. First, the structural design from the prior work is revisited, and three issues related to practical application of this design are explored. Next, two-dimensional CFD analysis is performed on the CTEF design to generate aerodynamic performance data as a function of actuation voltage, airspeed, and angle-of-attack. This data is then used within a comprehensive analysis of a swashplateless rotor system to investigate the effectiveness of CTEFs for primary flight control. Results show that the CTEF provides ample control authority, and that a CTEF-controlled helicopter may be a feasible concept given sufficient additional research effort and resources.

CTEF STRUCTURAL DESIGN

The CTEF concept utilizes a tapered bimorph design and off-the-shelf Macro-Fiber Composite (MFC) actuators (ref. 11), as presented in reference 3. Prior work on the CTEF concept focused on developing the coupled analysis tools needed to analyze a rotor blade cross-section with a CTEF, and verifying that the CTEF could produce useful deformation and control authority in the presence of aerodynamic pressure. To facilitate this initial analysis, a number of assumptions were made that have since been verified. This section will discuss three of these assumptions and how they relate to the performance of a practical CTEF cross-section. First, a practical design for joining the CTEF bimorph to the primary spar is presented and compared to the ideal boundary condition assumption. Next, the effect of MFC bias voltage on the bimorph actuation is examined. Finally, the performance of the CTEF as it is scaled to larger chord lengths is discussed.

The CTEF cross-sectional design presented in this work is an optimized design based on the tapered 4-ply bimorph design presented in reference 3. The design uses a 9.84-in.-chord VR-18 airfoil with four layers of MFC actuators on each side of the trailing edge bimorph, which starts at 0.50c. The airfoil regions above and below the bimorph are filled with a Nomex honeycomb and covered with a nylon skin. The bimorph has an E-glass fabric core separating the upper and lower layers of MFCs, which tapers from a thickness of 0.0945 in. at 0.50c to zero at 0.76c. This core and the bimorph can be observed in the cross-sectional layout presented in figure 1.

The deformation that is produced by this CTEF design during actuation is presented in figure 2. The quasi-static deformation presented is for Mach 0.65 at zero angle-of-

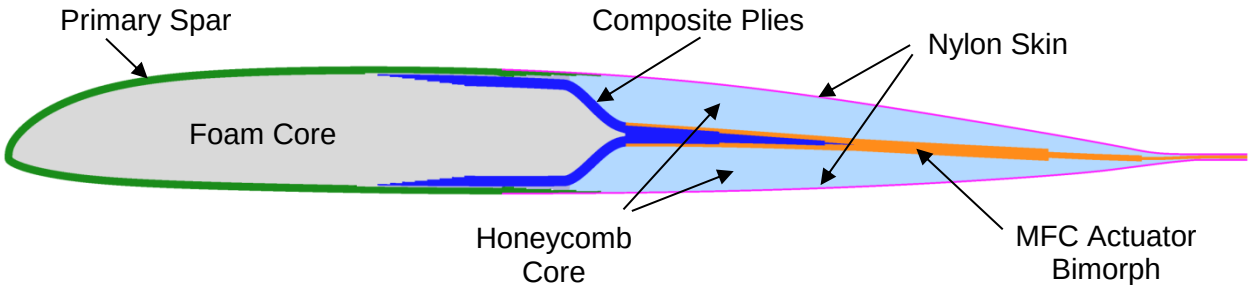

Figure 1. Cross-sectional view of the developed CTEF design.

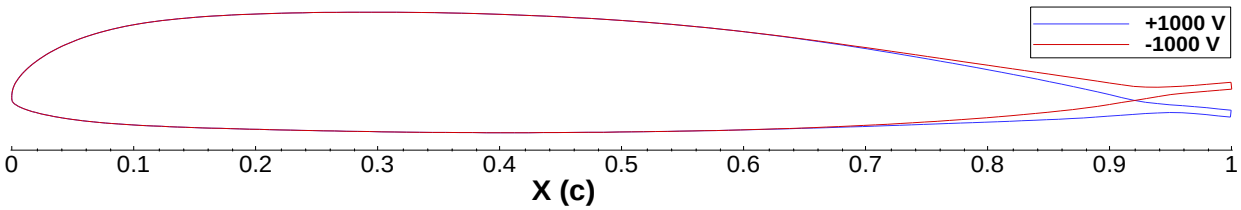

Figure 2. Deformed airfoil shape of the developed CTEF design at Mach 0.65.

attack. The downward deflection at +1000V is -0.135 in., and the upward deflection at -1000V is 0.0996 in. Although these deflections appear small, CFD studies indicate that they generate a range in lift coefficient, C_L, of 0.534, and a range in pitching moment coefficient, C_M, of 0.100 at M = 0.65 and $\alpha = 0°$.

Manufacturable Design

Most of the prior work performed to identify optimal bimorph geometries used a 1-D solution algorithm coupled to an XFOIL (ref. 12) aerodynamic analysis to compute the deformation of the cross-section during bimorph actuation. Comparison with NASTRAN finite-element analysis of the cross-section demonstrated that the 1-D algorithm was reasonably accurate, but both analysis methods assumed that the root of the bimorph had an ideal cantilevered boundary condition. A method for attaching the bimorph to the primary load-bearing spar has been developed and is presented in figure 1. Rotor blades typically use a closed-section spar to provide sufficient axial strength and torsional stiffness. A simple cantilevered connection between a basic bimorph and the aft end of the spar would not have sufficient stiffness or strength to transfer the aerodynamic loads from the bimorph to the spar. The proposed design utilizes the presence of the non-active core within the tapered bimorph to connect the bimorph to the spar and transfer the aerodynamic loads. The primary spar is manufactured with a tongue that extends aft from the spar, and this tongue forms the non-active core of the tapered bimorph. In the case of a composite structure, such as the design presented in figure 1, composite plies sweep aft from the upper and lower surfaces to join and form the core of the tapered bimorph. These composite plies are then bonded to a C-shaped spar to form the closed section needed to meet the requirements for torsional rigidity.

To compare the performance of the new CTEF cross-sectional design with the 1-D analysis used to optimize the cross-section, a NASTRAN finite-element mesh of the new CTEF design was created. The NASTRAN analysis (SOL 101) uses the same XFOIL aerodynamic analysis as the 1-D structural analysis. The results of this analysis are summarized in Table 1. With no aerodynamic forces on the cross-section, a +1000V actuation voltage results in a predicted trailing-edge deflection of -0.224 in. (trailing edge down) for the 1-D analysis with ideal bimorph boundary conditions, and a trailing-edge deflection of -0.219 in. for the NASTRAN analysis of the as-designed cross-section. At a velocity of Mach 0.65 and a 0° angle-of-attack, the 1-D analysis predicts trailing-edge deflection of -0.135 in., +0.295 ΔC_L, and -0.0546 ΔC_M for a +1000V actuation voltage. The NASTRAN analysis of the as-built cross-section predicts trailing-edge deflection of -0.122 in., +0.287 ΔC_L, and -0.0548 ΔC_M. Thus, the 1-D analysis overpredicts the performance of the CTEF by approximately 3 percent, which is only slightly greater than the difference presented in reference 3, between the 1-D analysis and NASTRAN models with ideal boundary conditions at the root of the bimorph. The method of transitioning the aft end of the primary spar into the core of the bimorph therefore seems to be very effective at transferring load to the spar without a significant loss in CTEF performance.

Table 1. Comparison of CTEF deflection and aerodynamic performance between the 1-D analysis and NASTRAN analysis of the as-designed cross-section.

No aero loads, +1000 V Actuation		
	1-D Analysis	As-designed
Tip deflection (in.)	-0.224	-0.219

Mach 0.65, 0° angle-of-attack, +1000 V Actuation		
	1-D Analysis	As-designed
Tip deflection (in.)	-0.135	-0.122
ΔC_L	0.295	0.287
ΔC_M	-0.0546	-0.0548

Bias Voltage

Analysis performed in previous research efforts has assumed a maximum actuation voltage of ±1000V. Thus, a +1000V actuation assumed that the MFCs on the upper half of the bimorph were actuated at +1000V and those on the lower half were actuated at -1000V to deform the cross-section. MFCs, however, have an actuation range of -500V to +1500V. It is therefore necessary to use a +500V bias voltage in order to achieve a ±1000V actuation range.

Table 2. Comparison of CTEF deflection and aerodynamic performance at Mach 0.65 with and without a bias voltage.

No bias voltage				+500 V bias voltage			
V_{upper}/V_{lower}	Tip deflection (in.)	C_L	C_M	V_{upper}/V_{lower}	Tip deflection (in.)	C_L	C_M
+1000/-1000	-0.135	0.424	-0.0570	+1500/-500	-0.133	0.421	-0.0565
-1000/+1000	0.100	-0.110	+0.0433	-500/+1500	0.097	-0.1067	+0.0428
0/0	-0.017	0.157	-0.0068	+500/+500	-0.016	0.155	-0.0066

Analysis has been performed that shows that the use of a bias voltage does not significantly affect the performance of the CTEF. Examples of these results are presented in Table 2 for the 1-D analysis of the CTEF design for a velocity of Mach 0.65 and a zero angle-of-attack. These results display a difference of less than 2 percent between the cases with and without the +500V bias voltage. It is interesting to note that the performance of the cases with the bias voltage was consistently less than the cases without. The +500V bias voltage is believed to induce an extensional strain, which results in a small nonlinear stiffening of the bimorph and slightly reduces the deformation of the CTEF during actuation.

Scaling Effects

The cross-sectional analysis presented in this work and in reference 3 was performed using a 9.84-in.-chord airfoil. This size is comparable to the rotor blades found on light helicopters, and it was chosen based on the desire to manufacture a full-scale CTEF test article without the requirement for the development of custom actuators. An area of concern for the CTEF concept is whether the CTEF cross-sectional design can be readily scaled to larger blade sizes. Analysis has been performed to demonstrate that when the entire cross-section is geometrically scaled up or down with no change in air speed, the CTEF deflection and the aerodynamic control authority remain unchanged. This insensitivity to scale results from the fact that the force generated by the MFCs and the aerodynamic forces are both linearly proportional to the chord, so the deformation of the cross-section and the internal strains do not change as the size increases.

In practice, however, the cross-sectional geometry cannot typically be exactly scaled from one size to another. This inconsistency with the ideal result is primarily because the designer is limited by the discrete thicknesses of the available composite materials and the MFC actuators. MFC actuator length is an issue, as well. The current CTEF design is based on a stock MFC actuator length of 3.35 in. (Model M-8557-P1), so if this design is scaled up or down, the design would have to use custom actuator sizes or the cross-sectional layout of the actuators would have to be redesigned.

Scaling to larger chord lengths is less challenging than scaling to smaller chord lengths, and has the benefit of giving more flexibility with which to optimize the structural design variables. For example, when the current design is scaled from 9.84 in. chord to 20.75 in., eight 0.012-in.-thick MFC actuators must be positioned within the design rather than just four. One would expect that a more optimal design would be possible in this case; however, the performance improvements that are possible have been shown to be minimal. Optimization of the CTEF design with a chord of 20.75 in. and a proportionally similar quantity of MFC actuators was performed to demonstrate the gains that are possible in large rotor blades. These results are presented in Table 3. At a velocity of Mach 0.65 and a 0° angle-of-attack, +1000V actuation results in a design where the trailing-edge deflection is -0.0148c (-0.307 in.) as opposed to -0.0137c (-0.135 in.) for the 9.84-in-chord design. Similarly, this deformation corresponds to +0.311 ΔC_L and -0.0561 ΔC_M, as opposed to +0.295 ΔC_L and -0.0546 ΔC_M for the 9.84-in.-chord design. Based on this result, performance estimates obtained from analysis of the 9.84-in-chord CTEF design have been used in this work as a conservative design for the initial characterization and comprehensive analysis of a rotor using CTEFs for primary flight control.

Table 3. Scaling of CTEF deflection and aerodynamic performance. M = 0.65, α = 0°, +1000 V actuation.

	9.84-in. chord	20.75-in. chord
Tip deflection (c)	-0.0137	-0.0148
ΔC_L	0.295	0.311
ΔC_M	-0.0546	-0.0564

CTEF AIRFOIL TABLE DEVELOPMENT

The development of high quality two-dimensional aerodynamic tables is a key step to modeling the CTEFs in a comprehensive rotorcraft analysis. The CTEF aerodynamic performance has been validated using

multiple analyses, initially with XFOIL, then with the more resource-intensive computational fluid dynamic (CFD) solutions TURNS, OVERFLOW, and FUN3D (ref. 1). The reason for using multiple aerodynamic codes was to assess the modeling fidelity and accuracy that is required to properly couple the aerodynamic forces and moments with the structural model. There are two resulting outputs from the various aerodynamic methods. The first is a pressure distribution over the airfoil that is interpolated onto the structural model to determine the amount of deflection the CTEF produces under an aerodynamic load. All of the aerodynamic codes result in a similar pressure distribution towards the trailing edge of the airfoil, which is the critical location for calculating accurate deflections. The second result from the aerodynamic analyses is the total lift, drag, and pitching moment coefficients for the airfoil. Because the aerodynamic performance coefficients require accurate pressure distributions over the leading edge of the airfoil, the higher fidelity CFD methods result in more consistent and accurate performance coefficients than does XFOIL. XFOIL was found to be useful, however, since it provides almost instantaneous solutions compared to the CFD methods. Using XFOIL permits a first order approximation for the airfoil pressure distribution so that trailing edge deflections may be calculated quickly, permitting timely optimization of the CTEF design for maximum control authority (ref. 3).

To obtain high quality aerodynamic coefficients, however, CFD methods are required. FUN3D (ref. 13) was chosen to develop the two-dimensional airfoil tables for use in the comprehensive analysis. For discrete flaps, a family of tables would be developed as a function of flap angle. Since the CTEF does not produce specific, identifiable flap angles like a discrete flap, the tabulated CTEF airfoil data is stored as a function of actuation voltage rather than flap angle. The airfoil tables were created using FUN3D with a 2D airfoil mesh, and a combination of steady state and time-accurate solutions. The time-accurate solutions were required because this study examined a larger angle-of–attack range and higher speeds than were analyzed during the optimization study of reference 3, making it necessary to model the unsteady aerodynamics due to stall and transonic effects. During the development of the airfoil tables, the structural code generates the profile of the airfoil, including the deformation produced by the bimorph. This profile is then used by an automatic mesh generator to create the CFD mesh, the aerodynamic analysis is run, and the resulting pressure distribution is applied to the structural analysis for recalculation of the airfoil profile. The steady state solution restarts with a new mesh every coupled analysis iteration. The time-accurate solution restarts with a deformation profile provided to FUN3D and FUN3D deforms the current mesh. This permits the new calculations to restart from the previous iteration. Using this approach, computational time is saved by eliminating

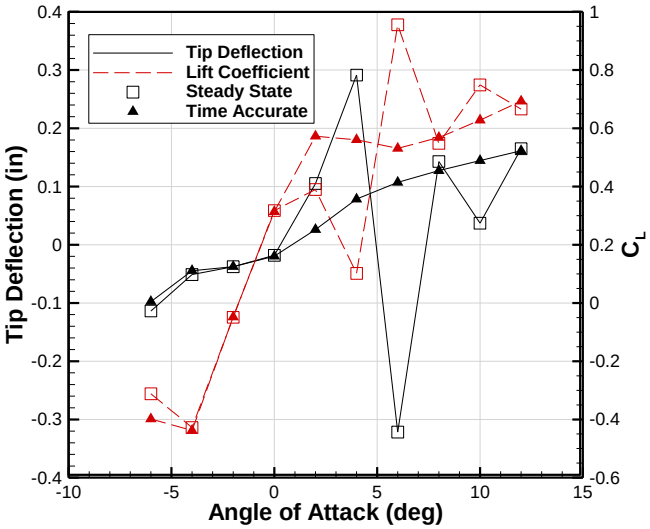

Figure 3. Deflection and coefficient of lift versus angle of attack for the steady state and time accurate solutions, at Mach 0.75 and 0V actuation.

large startup transients associated with the time-accurate solutions during each iteration. Both the steady state and time-accurate solution methods iterate with the structural solution until a fluid-structural convergence criterion is met.

The steady state solution was not found to be accurate at high speeds ($M \geq 0.7$) and in the stall regions of the operational envelope of the airfoil due to the unsteady nature of the aerodynamics. An example is provided in figure 3, which presents the unactuated deflection and coefficient of lift for the steady state and time-accurate solutions at M = 0.75. The time-accurate solution permits a time-averaged pressure distribution to be computed so that the net effects of the unsteady aerodynamics are captured. Since the steady state solution is unable to model the time-dependent characteristics of turbulence, it does not converge and the pressure distribution provided to the structural code is inaccurate.

Figure 4 presents examples of the airfoil table fidelity for the unactuated, high speed cases. Speed ranges from Mach 0.7 to 0.9 for angles of attack from -6 to +12 degrees are presented. Mach 0.9 clearly exhibits transonic effects, which result in large increases in the drag and changes in pitching moment coefficients.

Figure 5 presents sample CTEF control authority for a range of actuation voltages. The lift, drag, and pitching moment coefficients are presented for a range of angles of attack and CTEF actuation voltages at M = 0.3. The control authority is relatively constant with a ΔC_L of 0.7 and ΔC_M of 0.12 over a useful range of angles of attack. The asymmetric shape of the airfoil causes the drag to increase dramatically at negative angles of attack and contributes to the asymmetric pitching moment coefficients.

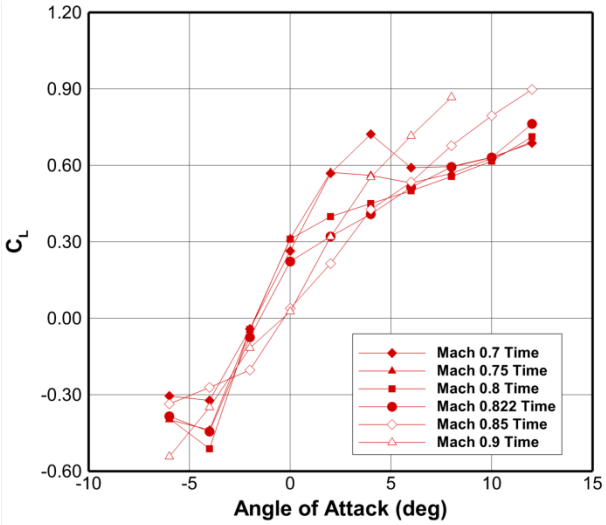

(a) Lift coefficient.

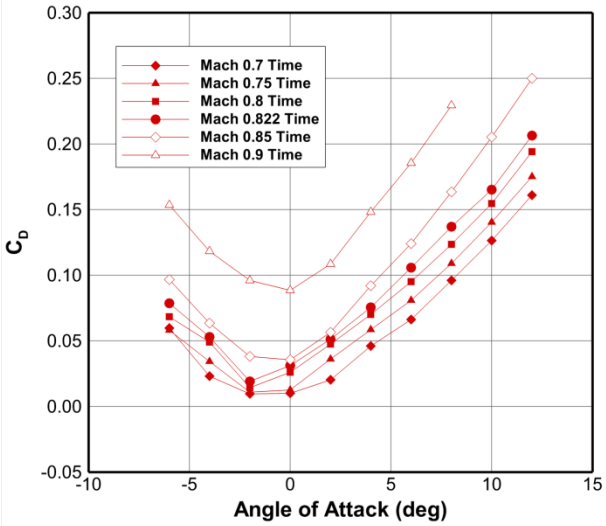

(b) Drag coefficient.

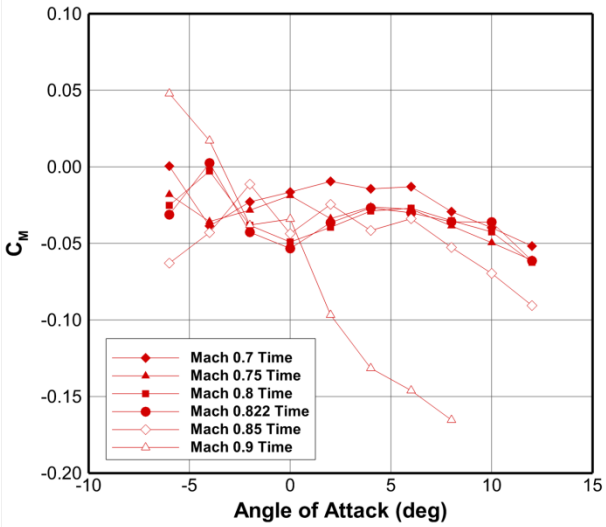

(c) Pitching moment coefficient.

Figure 4. CFD results for the time accurate solution for the unactuated CTEF airfoil.

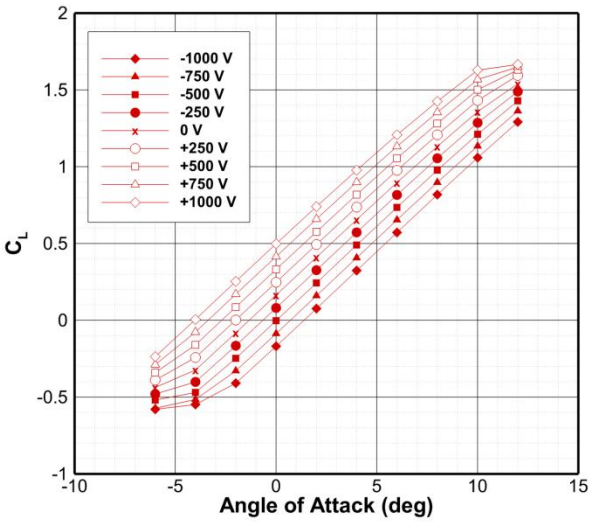

(a) Lift coefficient.

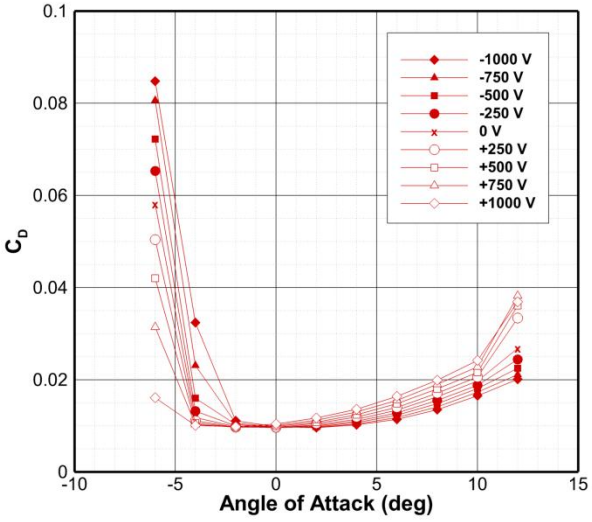

(b) Drag coefficient.

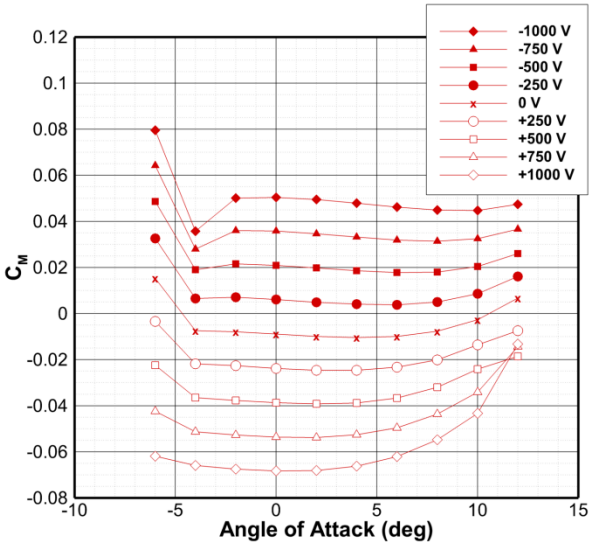

(c) Pitching moment coefficient.

Figure 5. CFD-generated airfoil characteristics of CTEF for various actuation voltages, M = 0.3.

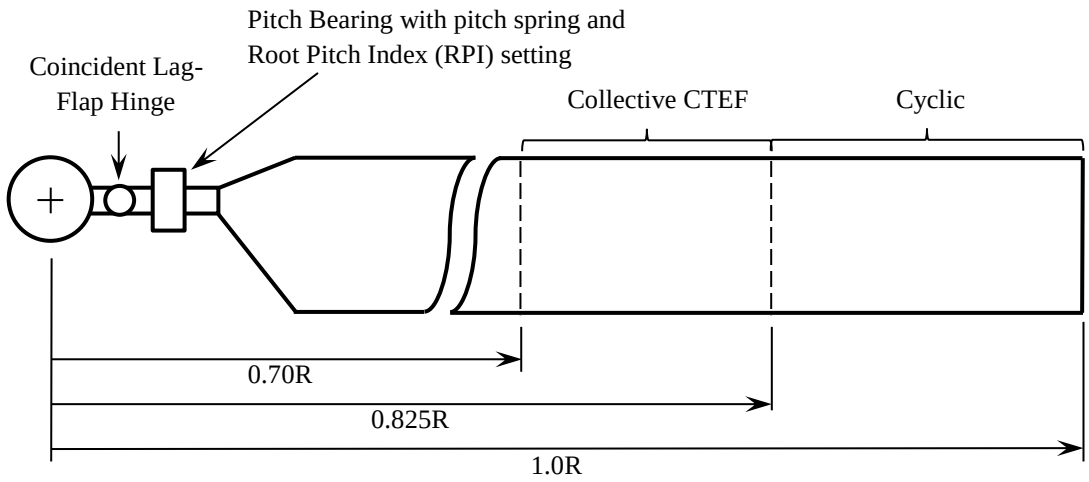

Figure 6. CAMRAD II model configuration.

Table 4. Helicopter and rotor properties.

Helicopter Properties	
Weight (lb)	16,800
CG station (ft)	0
CG waterline (ft)	5.82
Equivalent flat plate area (ft^2)	22.56
Horizontal tail ($d(L/Q)$)/α (ft^2/rad)	269.4
Horizontal tail station (ft)	29.91
Main rotor properties[a]	
Rotor type	Articulated
Blade airfoil section	VR-18
Rotor radius (ft)	26.8
Number of blades	4
Solidity	0.082
Root pitch spring stiffness (ft-lb/rad)	1161
Tip Mach number	0.65
Linear blade twist (deg)	-18
Root cutout	0.15*R*
Flap hinge location	0.05*R*
Lag hinge location	0.05*R*
Pitch bearing location	0.051*R*
Flap frequency (/rev)	1.03
Lag frequency (/rev)	0.27
Tail rotor properties	
Blade airfoil section	NACA-0012
Rotor radius (ft)	5.5
Number of blades	4
Solidity	0.188
Tail rotor station (ft)	32.82
Rotor waterline (ft)	-0.81
Rotational speed ratio	5

[a]Blade center of gravity, aerodynamic center, and pitch axis are located at 0.25*c*.

COMPREHENSIVE ANALYSIS MODEL

A CAMRAD II (ref. 14) model of a utility-class helicopter in free flight was developed to examine the applicability of CTEFs as primary rotor flight control devices. The current model was based on the model developed to analyze discrete trailing-edge flap control in references 9 and 10. The general properties of the flight vehicle are provided in Table 4. Vehicle drag, including that of the main rotor hub, was modeled as an equivalent flat plate whose drag is assumed to act at the vehicle center of gravity. The locations of all vehicle components are measured with respect to the main rotor hub, where offsets are positive down and aft. A rectangular blade planform, uniform blade structural properties, and no kinematic blade pitch-flap coupling were assumed.

The general configuration of the main rotor is presented in figure 6, in which the location of the CTEFs and the relative location of the flap and lag hinges and the pitch bearing are shown. For efficient primary flight control, the pitch bearing must have a spring stiffness such that the fundamental blade torsion frequency is near 2/rev, and a root pitch index (RPI), defined as the pitch of the blade under an unloaded, nonrotating condition, must be employed as an offset to the spring. For this study the optimal root pitch spring stiffness (1161 ft-lb/rad) identified in references 9 and 10 was used, and RPIs in the range of +23 deg to +34 deg were examined. The radial extent of the CTEFs was chosen based on control authority requirements observed during initial exploratory analyses. The CTEF regions, although adjacent to one another, are not considered to impact each other from a structural displacement perspective. Therefore, the analysis produces results as if the trailing edge was sliced chordwise to permit unrestricted CTEF displacement, and there are discrete changes in airfoil lift and pitching

moment across the CTEF interfaces. While not strictly a realistic model of the continuous nature of the CTEF concept, the intent of the study is to determine whether sufficient control authority exists to justify further research activities.

The aerodynamic model employed is the standard CAMRAD II lifting-line wing using two-dimensional airfoil table look-up. Multiple CFD-generated airfoil tables were developed for application to the CTEF region to simulate CTEF deflection as a function of angle of attack, Mach number, and applied voltage in the range of -1000V to +1000V. CAMRAD II core modeling was used to disconnect the conventional swashplate and pitch bearing control, and connect the pilot collective pitch and longitudinal and lateral cyclic pitch controls to the CTEFs to achieve primary flight control simulations. Standard CAMRAD II corrections for unsteady aerodynamic response and yawed-flow effects were enabled throughout the study. No other specific modifications were made to the solution procedure to account for CTEF control versus conventional control.

COMPREHENSIVE ANALYSIS RESULTS

Analyses were conducted from low-speed forward flight to 150 kts (μ = 0.02 to 0.35). These analyses studied the impact of model fidelity, in terms of structural dynamics and inflow/vortex wake models, and blade RPI on CTEF control authority requirements, as these were the parameters that were determined to have the greatest effect on the results. Some of the analysis results for the rigid blade model with free wake failed to converge (fig. 9), but most of these instances are concentrated near the highest flight speeds. The failure to converge was not found to be associated with any physical phenomenon associated with the CTEF primary flight control concept, but instead from numerical convergence issues within the analysis framework. With additional effort most of these flight conditions could be demonstrated to work, however, doing so would not significantly impact the conclusions of the studies. Therefore, some limited flight speed ranges are evident within the results.

Figures 7 through 10 present the CTEF control authority requirements to achieve 1g forward-flight of the 16,800-lb flight vehicle. Each figure is presented in four parts. Part (a) presents the collective CTEF control authority in terms of the voltage requirement for the MFC actuators; part (b) the lateral cyclic requirement; part (c) the longitudinal cyclic requirement; and part (d) represents the magnitude of the total cyclic control authority requirement. This total cyclic component represents the maximum cyclic CTEF voltage amplitude required to achieve trimmed flight. As presented, the selection of RPI impacts the collective CTEF control requirements the most significantly, although the total cyclic control authority requirement is also affected by the selection of RPI, particularly in the range of μ = 0.10 to 0.35. Figures 7 through 10 examine the impact of the fidelity of the comprehensive model solution from least complex to most complex.

Figure 7 presents the CTEF control authority requirements for a rigid blade model with uniform inflow, and is comparable in model complexity to that presented in references 9 and 10. As presented, the collective control requirement (fig. 7(a)) is affected significantly by the choice of RPI, and achieving trim at the lowest RPIs exceeds the range of control authority available. Although the sensitivity of the collective control voltage requirements changes somewhat with flight speed, an approximate sensitivity is 125V per degree of RPI. Thus, a change in RPI of just a few degrees can make the difference between successful trim and failure due to a lack of sufficient control authority. The lateral cyclic (fig. 7(b)) control authority requirement is observed to be mostly independent of RPI, however, the longitudinal cyclic (fig. 7(c)) control authority requirement is observed to be moderately impacted by the selection of RPI, with a range of sensitivities as high as 60V per degree of RPI at the highest flight speeds. The total cyclic control (fig. 7(d)) is the most instructive of the three cyclic sensitivity plots in that it defines the magnitude of the control voltage necessary to achieve trim. No cyclic CTEF voltage requirements in excess of 500V are required, indicating that the collective CTEF voltage requirement is the most significant driver with regard to design for primary flight control.

Figure 8 presents the CTEF control authority requirements for an elastic blade model with uniform inflow. The results are similar in character to those for the rigid blade model with uniform inflow presented in figure 7. The collective control requirement (fig. 8(a)), however, is observed to require a larger range of control than that for the rigid blade model with uniform inflow. For example, the voltage range for any single RPI curve in figure 7(a) spans approximately 850V, whereas the range in figure 8(a) spans approximately 1000V to 1150V. The sensitivity of collective control to RPI in figure 8(a) is observed to be approximately 100V per degree of RPI, resulting in a smaller voltage span across the RPI values even though the range within an individual RPI value increased. The longitudinal cyclic control requirement in figure 8(c) is observed to have reduced somewhat; however, an increase in the lateral cyclic control requirement (fig. 8(b)) results in a minor increase in the total cyclic (fig. 8(d)) control requirement, with the maximum control voltage required approaching 600V.

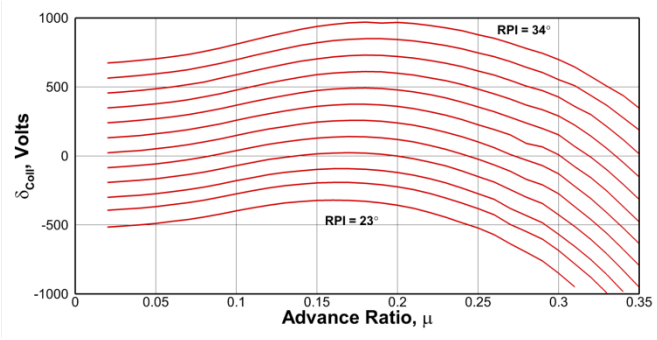

(a) Collective.

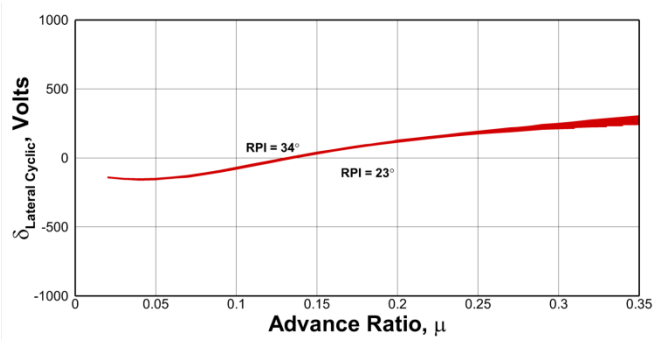

(b) Lateral cyclic.

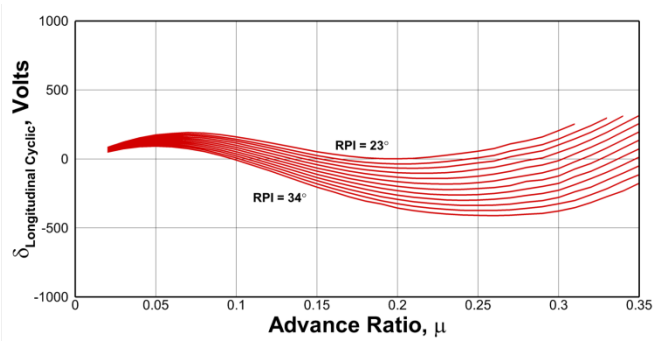

(c) Longitudinal cyclic.

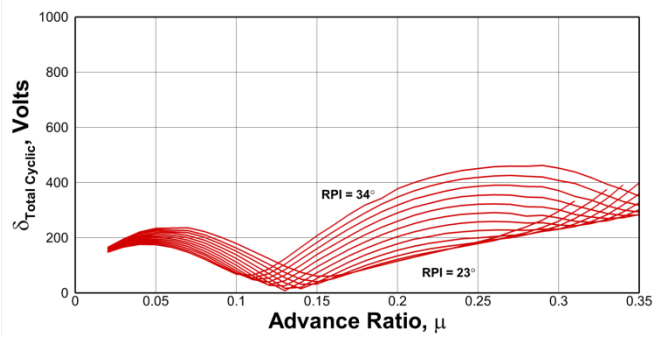

(d) Total cyclic.

Figure 7. CTEF control requirements as function of flight speed and root pitch index (RPI). Rigid blade model with uniform inflow. RPI presented in 1° increments.

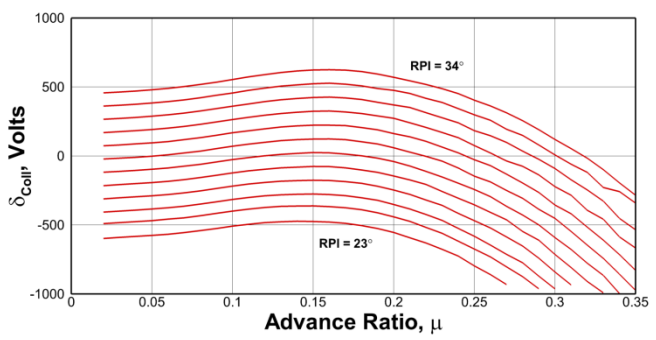

(a) Collective.

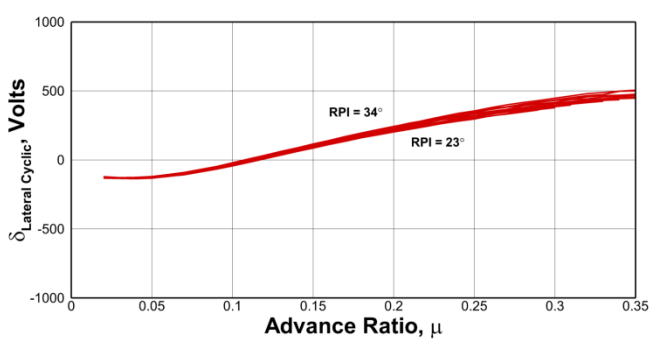

(b) Lateral cyclic.

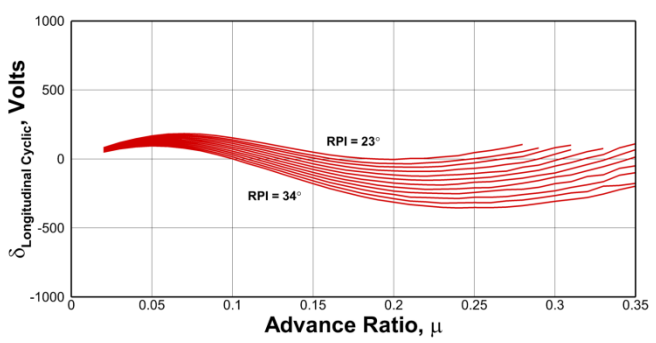

(c) Longitudinal cyclic.

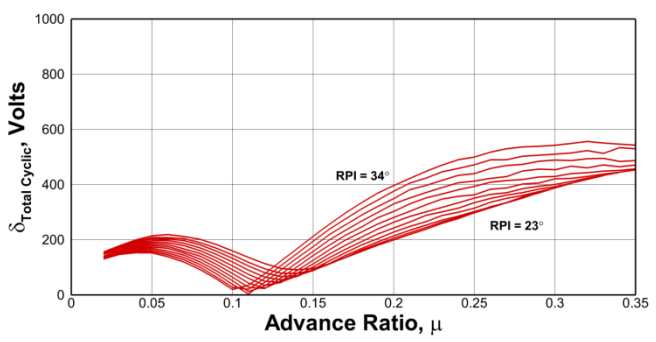

(d) Total cyclic.

Figure 8. CTEF control requirements as function of flight speed and root pitch index (RPI). Elastic blade model with uniform inflow. RPI presented in 1° increments.

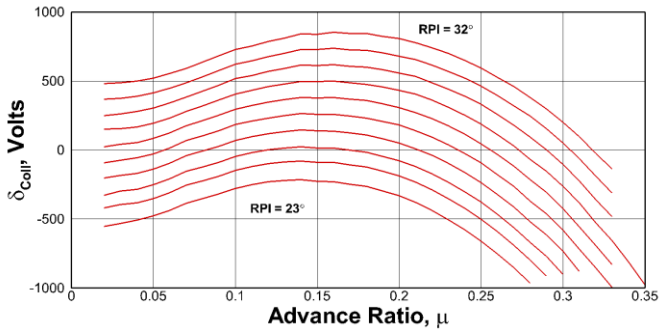

(a) Collective.

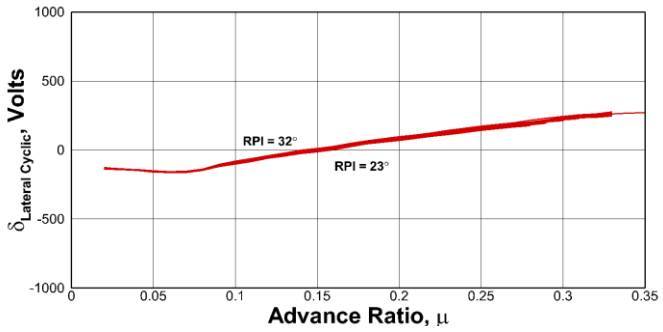

(b) Lateral cyclic.

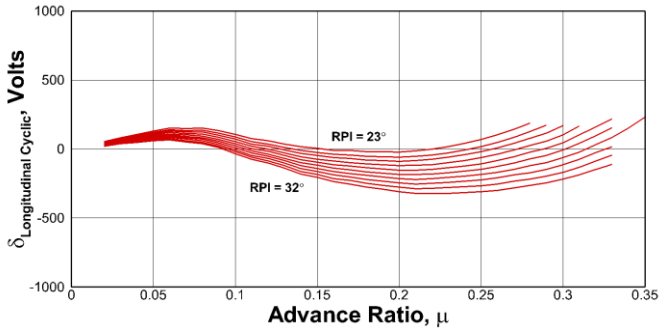

(c) Longitudinal cyclic.

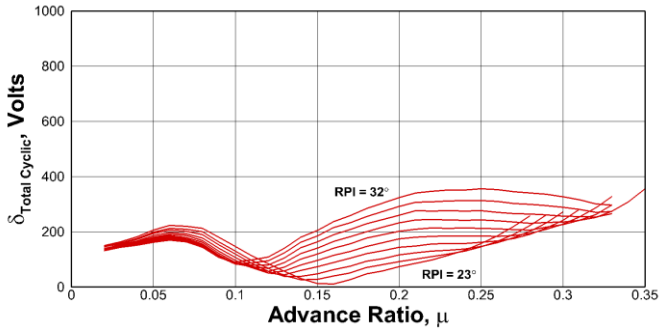

(d) Total cyclic.

Figure 9. CTEF control requirements as function of flight speed and root pitch index (RPI). Rigid blade model with free wake. RPI presented in 1° increments.

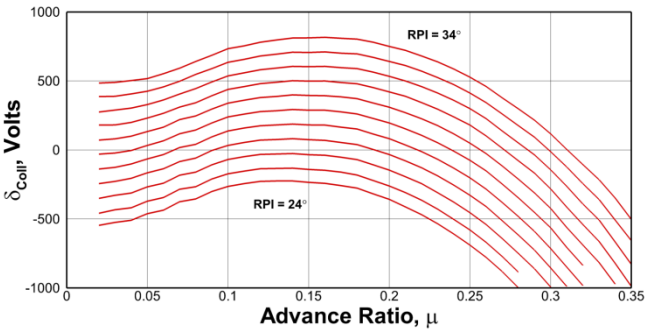

(a) Collective.

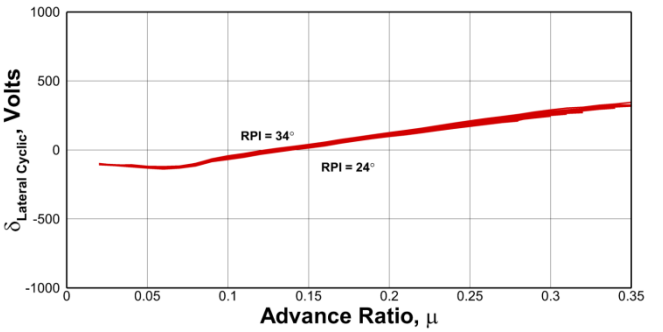

(b) Lateral cyclic.

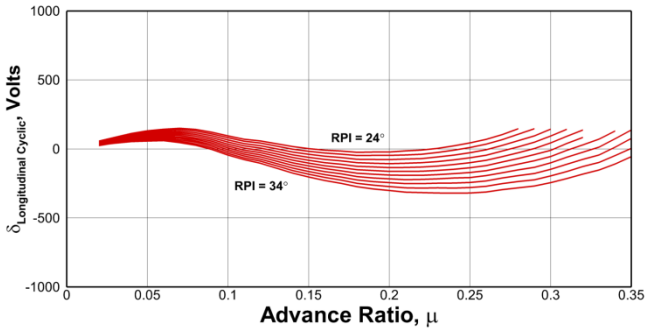

(c) Longitudinal cyclic.

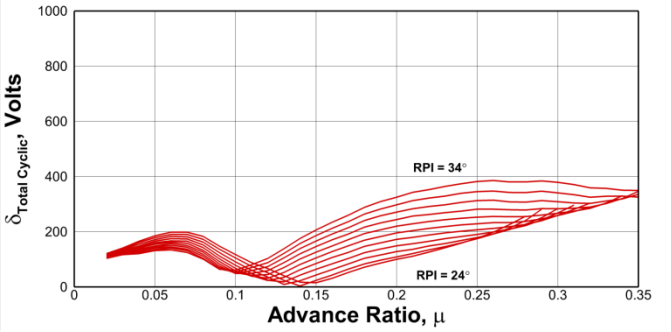

(d) Total cyclic.

Figure 10. CTEF control requirements as function of flight speed and root pitch index (RPI). Elastic blade model with free wake. RPI presented in 1° increments.

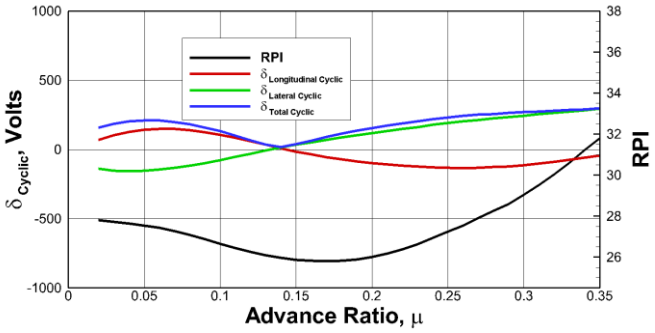

(a) Rigid blade with uniform inflow.

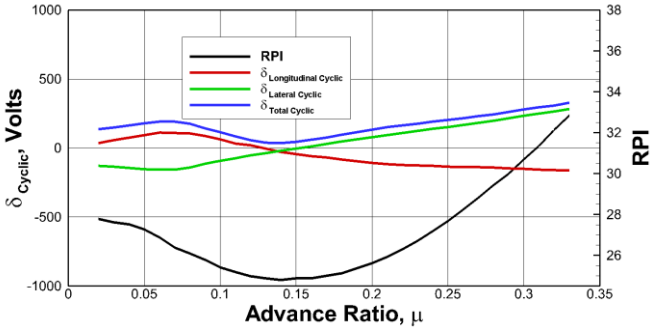

(b) Elastic blade with uniform inflow.

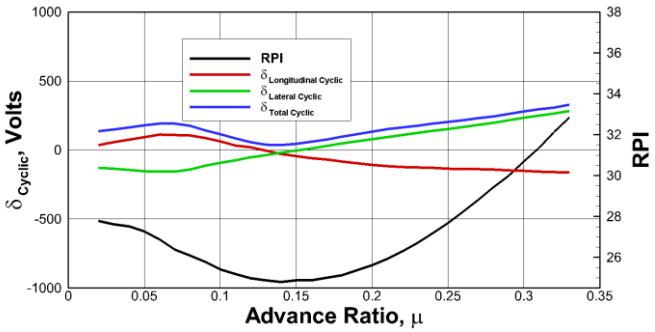

(c) Rigid blade with free wake

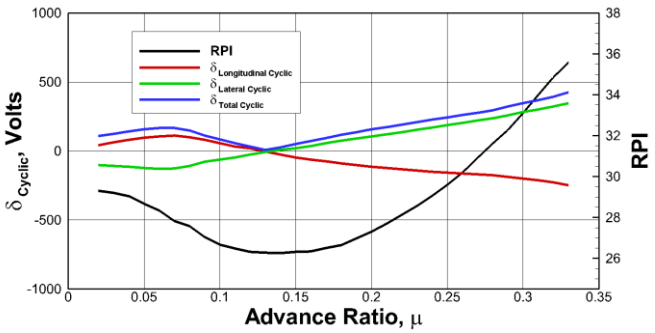

(d) Elastic blade with free wake.

Figure 11. Rotor configuration with RPI control and cyclic CTEF control.

Figure 9 presents the CTEF control authority requirements for a rigid blade with a free wake model. Again, the character of the results is not significantly different than the rigid or elastic blade models in uniform inflow presented in figures 7 and 8. The most significant results include the requirement for the collective CTEF voltage to span approximately 1500V throughout the flight speed range and that the range of total cyclic voltage requirements does not exceed 400V.

Figure 10 presents the CTEF control authority requirements for an elastic blade with a free wake model. The results are again similar in nature to those presented for the less complex models, with the total collective range spanning approximately 1500V and the total cyclic voltage requirement limited to 400V.

Examining figures 7 through 10, it becomes apparent that the complexity of the comprehensive model has relatively minor implications on the overall conclusions of the study. The study shows that primary flight control using CTEFs may be feasible, but that the largest driver with regard to success is the range of collective CTEF voltage required and the selection of an RPI that permits a full range of flight speeds within the control authority available. Further, it is reasonable to assume that when different gross weight configurations, density altitudes, and maneuver requirements are considered, that the required range of collective CTEF control authority will be extended further. While changing the relative spanwise extent and radial location of the collective and cyclic CTEFs could be used to reduce the collective CTEF voltage requirements somewhat, it is unlikely to be sufficient to achieve full flight control, and this approach would simply result in the requirement for the cyclic CTEF to work harder. Thus, a configuration in which the RPI is fixed is not likely to be successful in fulfilling all of the requirements necessary to achieve primary flight control on rotorcraft flight vehicles.

Based on these results, an alternative configuration is offered in which the RPI is incorporated as one of the vehicle primary flight controls. In such a configuration, a collective CTEF might be eliminated altogether or could be used to augment the RPI control, particularly in cases of maneuvering flight where a high rate of response is required. A study in which such a configuration was considered is presented in figure 11, in which RPI control is implemented for collective pitch control and a cyclic CTEF is used for cyclic control.

Figure 11 presents the results for the RPI control configuration for a rigid blade with uniform inflow (fig. 11(a)), an elastic blade with uniform inflow (fig. 11(b)), a rigid blade with free wake (fig. 11(c)), and an elastic blade with free wake (fig. 11(d)). Relatively little difference is observed in the results for the different fidelity models, although some differences in the range

and amplitude of the RPI are noted. Few significant differences are observed for the cyclic CTEF control, with none of the models indicating a requirement exceeding 500V of cyclic CTEF control.

Based on the results of the study, a configuration in which RPI control is incorporated into the primary flight control mechanism, perhaps with the aid of a collective CTEF, appears to be the best approach for implementing primary flight control with CTEFs. For such a configuration, helicopter 1g forward-flight trim is achieved with a cyclic CTEF spanning approximately 0.175R placed at the outermost portion of the blade, and requires less than 500V of cyclic CTEF actuation authority out of a limit of 1000V. Based on the results presented in reference 9, it is likely that typical maneuvering flight will be achievable with the remaining control authority available; however, additional studies need to be conducted for verification.

CONCLUSIONS

Analyses were conducted to study the potential for continuous trailing-edge flaps (CTEFs) to provide primary flight control of a helicopter. The CTEFs function using an optimized bimorph designed with Macro-Fiber Composite (MFC) actuators. Two CTEFs per blade are assumed radially on the outermost segments of the blade, with one CTEF configured to provide rotor collective pitch control and one CTEF configured to provide rotor cyclic control. The research conducted developed a practical design for joining the CTEF bimorph to the primary spar, studied the effect of MFC bias voltage on the bimorph actuation, and examined the performance of the CTEF as it is scaled to larger chord lengths. The development of a comprehensive analysis model to study primary flight control of a utility helicopter using CTEFs included the development of two-dimensional airfoil tables using computational fluid dynamics (CFD) methods. These airfoil tables included the effect of voltage applied to the CTEF through a structural analysis coupled to the CFD solution methods. Finally, the comprehensive rotorcraft model was used to evaluate the practicality of a CTEF-based flight control system of a helicopter.

Based on the results of this study, the following conclusions have been reached:

1. A practical and manufacturable design for the CTEF cross-section has been developed and shown to effectively transfer aerodynamic loads to the blade spar without significant loss in performance.

2. The use of a +500V bias voltage, which is necessary for full use of the MFC operating range, has been shown to not significantly affect the performance of the CTEF.

3. Scaling of the CTEF concept to other chord sizes does not significantly change the performance of the CTEF, provided that the individual material plies can be effectively scaled.

4. Collective control has been shown to be the most sensitive to the choice of blade root pitch index (RPI). Lateral cyclic control requirements are generally insensitive to the choice of RPI, and longitudinal cyclic control is moderately sensitive to the choice of RPI.

5. The choice of comprehensive model fidelity in terms of blades structural model (rigid vs. elastic) and inflow model (uniform inflow vs. vortex wake) does not significantly change the fundamental conclusions drawn in conclusion number 4.

6. Utilizing blade root pitch index control instead of or in addition to collective CTEF control provides a primary flight control solution that warrants further study.

FUTURE WORK

The results of the current investigation are sufficiently promising that additional research efforts are warranted. A bench test article of a 9.84-in.-chord CTEF section is under development for structural analysis validation and low-speed wind-tunnel testing for limited aero-structural interaction testing. Additional comprehensive analysis will study the incorporation of blade pitch-flap coupling, maneuver control authority and responsiveness of root pitch index and CTEF control, the use of higher-harmonic actuation to reduce vibration and noise, and seek to further develop a practical CTEF rotor design for primary flight control applications.

REFERENCES

1. Shen, J., Thornburgh, R., Kreshock, A., Wilbur, M., and Liu, Y., "Preliminary Design and Evaluation of an Airfoil with Active Continuous Trailing-Edge Flap," *AHS Future Vertical Lift Aircraft Design Conference*, San Francisco, California, January 18–20, 2012.

2. Grohmann, B., Muller, F., Achci, E., Pfaller, R., Bauer, M., Maucher, C., Dieterich, O., Storm, S., and Janker, P., "Design, Evaluation and Test of Active Trailing Edge," *American Helicopter Society 67th Annual Forum Proceedings*, Virginia Beach, VA, May 3–5, 2011.

3. Shen, J., Thornburgh, R., Liu, Y., Kreshock, A., and Wilbur, M., "Design and Optimization of an Airfoil with Active Continuous Trailing-Edge Flap," *American Helicopter Society 69th Annual Forum Proceedings*, Phoenix, Arizona, May 21–23, 2013.

4. Ormiston, R., "Aeroelastic Considerations for Rotorcraft Primary Control with On-Blade Elevons," *American Helicopter Society 57th Annual Forum Proceedings*, Washington, DC, May 9–11, 2001.

5. Shen, J., and Chopra, I., "A Parametric Design Study for a Swashplateless Helicopter Rotor with Trailing-Edge Flaps," *Journal of the American Helicopter Society*, Vol. 49, (1), January 2004, pp. 43–53.

6. Shen, J., Yang, M., and Chopra, I., "Swashplateless Helicopter Rotor with Trailing-Edge Flaps for Flight and Vibration Control," *AIAA/ASME/ASCE/AHS/ASC 45th Structures, Structural Dynamics, and Materials Conference Proceedings*, Palm Springs, CA, April 19–22, 2004.

7. Duling, C., Gandhi, F., and Straub, F., "On Power and Actuation Requirement in Swashplateless Primary Control Using Trailing-Edge Flaps," *American Helicopter Society 66th Annual Forum Proceedings*, Phoenix, AZ, May 11–13, 2010.

8. Shen, J., Chopra, I., and Johnson, W., "Performance of Swashplateless Helicopter with Trailing-Edge Flaps for Primary Flight Control," *Journal of the American Helicopter Society*, Vol. 55, (4), October 2010.

9. Sekula, M. and Wilbur, M., "Analysis of a Multi-Flap Control System for a Swashplateless Rotor." *Proceedings of the 67th Annual Forum of the American Helicopter Society*, Virginia Beach, Virginia, May 3 – 5, 2011.

10. Sekula, M., and Wilbur, M., "Analysis of a Multi-Flap Control System for a Swashplateless Rotor," *Journal of the American Helicopter Society*, Vol. 57, (3), July 2012.

11. Wilkie, W., Bryant, R., High, J., Fox, R., Hellbaum, R., Jalink, A., Little, B., and Mirick, P., "Low-cost Piezocomposite Actuator for Structural Control Applications," *Proc. SPIE 3991, Smart Structures and Materials 2000: Industrial and Commercial Applications of Smart Structures Technologies*, 323, Newport Beach, CA, June 2000.

12. Drela, M., "XFOIL: An Analysis and Design System for Low Reynolds Number Airfoils," Conference on Low Reynolds Number Airfoil Aerodynamics, University of Notre Dame, June 1989.

13. "FUN3D website," http://fun3d.larc.nasa.gov.

14. Johnson, W. CAMRAD II, Comprehensive Analytical Model of Rotorcraft Aerodynamics and Dynamics, Johnson Aeronautics, Palo Alto, California, 1994.